Insights into the K–Pg extinction aftermath: The Danish Cerithium Limestone Member

TJÖRDIS STÖRLING, ISALINE DEMANGEL, ANDERS LINDSKOG, JACOB ANDERSSON, MIKAEL CALNER, DANIEL J. CONLEY & SYLVAIN RICHOZ

Geological Society of Denmark
https://2dgf.dk

Received 12 January 2023
Accepted in revised form
10 July 2024
Published online
13 November 2024

Störling, T., Demangel, I., Lindskog, A., Andersson, J., Calner, M., Conley, D.J. & Richoz, S. 2024. Insights into the K–Pg extinction aftermath: The Danish Cerithium Limestone Member. Bulletin of the Geological Society of Denmark, Vol. 73, pp. 175–191. ISSN 2245-7070. https://doi.org/10.37570/bgsd-2024-73-10

The Cretaceous–Palaeogene (K–Pg) mass extinction about 66 Ma ago was one of Earth's largest mass extinction events. The demise of calcifiers, among others, influenced biogeochemical cycles and changed the conditions for carbonate deposition in the global ocean. This study addresses the sedimentology and carbonate microfacies of the Cerithium Limestone Member of the Rødvig Formation within the renowned Stevns Klint succession in Denmark. The limestone was deposited in the earliest Danian Stage, immediately after the K–Pg mass extinction. It is a pale yellow, partly cemented unit with a dense network of *Thalassinoides* burrows and numerous flint nodules. Studies of the thin sections revealed that the Cerithium Limestone Member is more variable than expected from its overall homogeneous appearance at the macroscopic scale. The thin sections and scanning electron microscope (SEM) images showed that the highly bioturbated limestone consists of four principal microfacies: a mudstone, a wackestone and two different packstones. The 30 to 120-cm thick Cerithium Limestone Member fills depressions between low-amplitude mounds in the Maastrichtian chalk. The lowermost part constitutes a thin layer of a bryozoan-rich packstone, probably reworked from the crests of the Maastrichtian mounds. The successive part of the member is dominated by wackestone with mainly foraminifera (planktic and benthic), molluscs and echinoderm debris, and in some areas an abundance of peloids. The foraminifera- and mollusc-rich packstone appears in lenses. The mudstone contains few foraminifera and is linked to burrows and syn-sedimentary fractures. SEM observations revealed that the Cerithium Limestone Member corresponds to a dispersed micrite, with small calcite crystals ~1–4 μm in size. The general shape of these calcite crystals suggests precipitation from cyanobacterial activity and, thus, a microbial genesis for the micrite of the Cerithium Limestone Member.

Keywords: Cerithium Limestone Member, Stevns Klint, Cretaceous–Palaeogene boundary, carbonate microfacies, thin sections, Danian, microbial micrite.

Tjördis Störling [tjordis.storling@geol.lu.se], Isaline Demangel [isaline.demangel@geol.lu.se], Anders Lindskog [anders.lindskog@geol.lu.se], Mikael Calner [mikael.calner@geol.lu.se], Jacob Andersson [ja0503an-s@student.lu.se], Daniel J. Conley [daniel.conley@geol.lu.se], Sylvain Richoz [sylvain.richoz@geol.lu.se], Department of Geology, Lund University, Sölvegatan 12, 223 62 Lund, Sweden.

The Cretaceous–Palaeogene (K–Pg) mass extinction at 66 Ma represents one of the five largest extinctions in the past 500 million years, with the disappearance of ~75% of marine species (e.g., Alvarez *et al.* 1980; Schulte *et al.* 2010). This extinction event was triggered by the impact of a large asteroid (e.g., Alvarez *et al.* 1980; Schulte *et al.* 2010; Hull *et al.* 2020) in the Yucatán Peninsula of Mexico (Fig. 1) and, within a broader time frame, by the massive Deccan flood basalt volcanism (e.g., Chenet *et al.* 2009; Schoene *et al.* 2019). It resulted in catastrophic changes of the Earth's climate and ecosystem disruptions (Schulte *et al.* 2010). In the marine realm, ocean acidification, darkening and cooling had a significant impact on primary producers (Hull *et al.* 2020), particularly calcifiers living in the photic zone (Olsson *et al.* 1999; Bown 2005; MacLeod *et al.* 2007; Bralower *et al.* 2020).

This disturbance of the food chain enabled the emergence of a new ecological equilibrium, with diatoms and dinoflagellates dominating over calcareous nannoplankton (Katz *et al.* 2004; Knoll & Follows 2016). Consequently, the carbon cycle underwent significant transformations (Birch *et al.* 2016), with changes in the export, burial and accumulation rates of organic carbon (e.g., Zachos & Arthur 1986; D'Hondt 2005; Henehan *et al.* 2016; Alvarez *et al.* 2019; Sepúlveda *et al.* 2019).

Extensive research has been conducted on the extinction interval, yet the understanding of the recovery processes in the earliest Paleocene has received less focus. Palaeontological and geochemical studies have provided an increasingly detailed record of the biotic and climatic/environmental development through the early Paleocene (e.g., Rasmussen *et al.* 2005; Gilleaudeau *et al.* 2018; Alvarez *et al.* 2019; Westerhold *et al.* 2020; Frederiksen *et al.* 2024). To date few detailed and systematic studies of the microfacies characteristics in thin sections from lower Paleocene strata have been published. Studies in sedimentology and carbonate microfacies can be used to better understand the sea-floor environment, including surface and intra-sediment processes, in the earliest aftermath of the K–Pg event. The coastal cliffs along Stevns Klint in south-eastern Denmark (Figs 1B, 2) provide an excellent succession that spans the upper Cretaceous to the lower Palaeogene (Fig. 3) and the opportunity to investigate the development of non-tropical carbonate depositional systems throughout this time interval. There, the Cerithium Limestone Member of the Rødvig Formation is found in the lowermost part of the local Palaeogene succession.

This study aims to clarify the genesis and palaeoenvironmental conditions of the deposition of the limestone by providing a detailed analysis of the microfacies and microfossil content of the Cerithium Limestone Member in the Rødvig section of Stevns Klint.

Geological setting and stratigraphy

Stevns Klint is a 14.5 km long coastal cliff in eastern Denmark (Fig. 2A). The cliffs rise up to 20 m above sea level, and the exposed succession exhibits the transition from the white chalks of the Maastrichtian (*c.* 72–66 Ma) to the bryozoan-rich mounds of the lower Danian (e.g., Surlyk 1997; Hart *et al.* 2005; Surlyk *et al.* 2006). The Stevns Klint succession (Fig. 3) is well known for the iridium anomaly documented by a thin but distinct clay bed known as the Fiskeler Member (Rødvig Formation), which gave rise to the hypothesis that an asteroid impact caused the mass extinction at the K–Pg boundary (Alvarez *et al.* 1980).

The Maastrichtian chalk of the Møns Klint Formation is divided into the Sigerslev Member and the Højerup Member (Fig. 3). The Sigerslev Member corresponds to a white mound-bedded chalk (Surlyk *et al.* 2006), which is exposed to a maximum of 32 m along the cliff. The overlying unit, the Højerup Member, is a 4–5 m thick bryozoan-rich grey chalk of the uppermost Maastrichtian (Surlyk *et al.* 2006). The lower Danian limestones are subdivided into two formations: the Rødvig Formation with the Fiskeler and the Cerithium Limestone members, and the Ste-

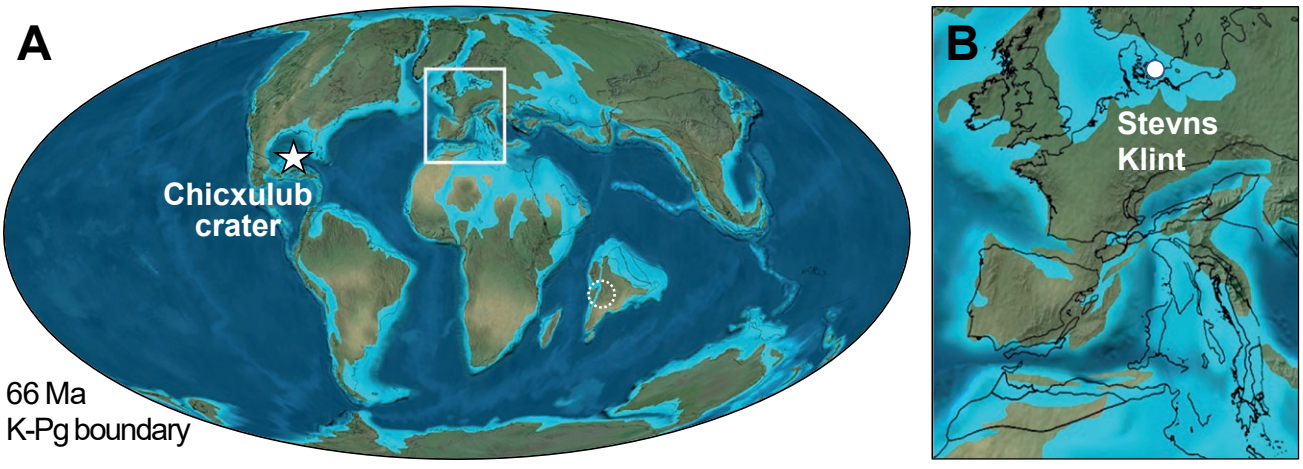

Fig. 1. Palaeogeographical maps during the Cretaceous–Palaeogene boundary interval (*c.* 66 Ma). **A**: Global palaeogeographical reconstruction with the Chicxulub impact site (white star) and the Deccan traps (white, dashed line). **B**: Map of the palaeogeography of Europe with the study site at Stevns Klint (white dot, palaeolatitude 44.53°N). Green: land, light blue: shallow seas, dark blue: open oceans. © 2016 Colorado Plateau Geosystems Inc. Modified from Sepúlveda *et al.* (2019).

vns Klint Formation with the Korsnæb Member (Fig. 3). The Danian Fiskeler Member with the iridium anomaly at its base (Alvarez *et al.* 1980), is a stratified clay-marl layer typically 5–10 cm thick lying just above the K–Pg boundary (e.g., Surlyk *et al.* 2006). It reaches a maximum thickness of ~ 45 cm at Kulstirenden in the northern part of Stevns Klint (Hart *et al.* 2005; Fig. 2B). This thin unit passes gradually or, in certain places, abruptly upwards into the lower Danian Cerithium Limestone Member (Surlyk *et al.* 2006; Rosenkrantz *et al.* 2021).

The sampling location for the present study, called the Rødvig section, is situated at the southern end of Stevns Klint, immediately east of Rødvig at Korsnæb (55.25403°N, 12.39624°E; Fig. 2B).

The Cerithium Limestone Member

The Cerithium Limestone Member is named after the gastropod genus *Cerithium* (Forchhammer 1825). Despite numerous studies (e.g., Forchhammer 1825; Nielsen 1917; Rosenkrantz 1924; Bernecker & Weidlich 2005; Heinberg 2005; Machalski & Heinberg 2005; Surlyk *et al.* 2006; Gilleaudeau *et al.* 2018; Rosenkrantz *et al.* 2021) the depositional conditions of the Cerithium Limestone Member are not completely understood.

The Cerithium Limestone Member has a typical thickness of about 30–60 cm (Surlyk *et al.* 2006). In northern sections, such as Korsnæb and Kulstirenden, its thickness can reach up to 80 cm and 120 cm, respectively (Hart *et al.* 2005; Surlyk *et al.* 2006). A dense network of *Thalassinoides* burrows and flint nodules in the upper part form a striking characteristic of the unit (Surlyk *et al.* 2006). The *Thalassinoides* burrows are concentrated horizontally and form an important local marker horizon below a syn-sedimentary hardground (e.g., Ekdale & Bromley 1984; Surlyk 1997). This hardground surface reflects a fall in sea level coupled with submarine erosion and a hiatus (e.g., Rosenkrantz 1924; Surlyk *et al.* 2006). The prominent erosion surface truncates both the Cerithium Limestone Member and the crests of the Maastrich-

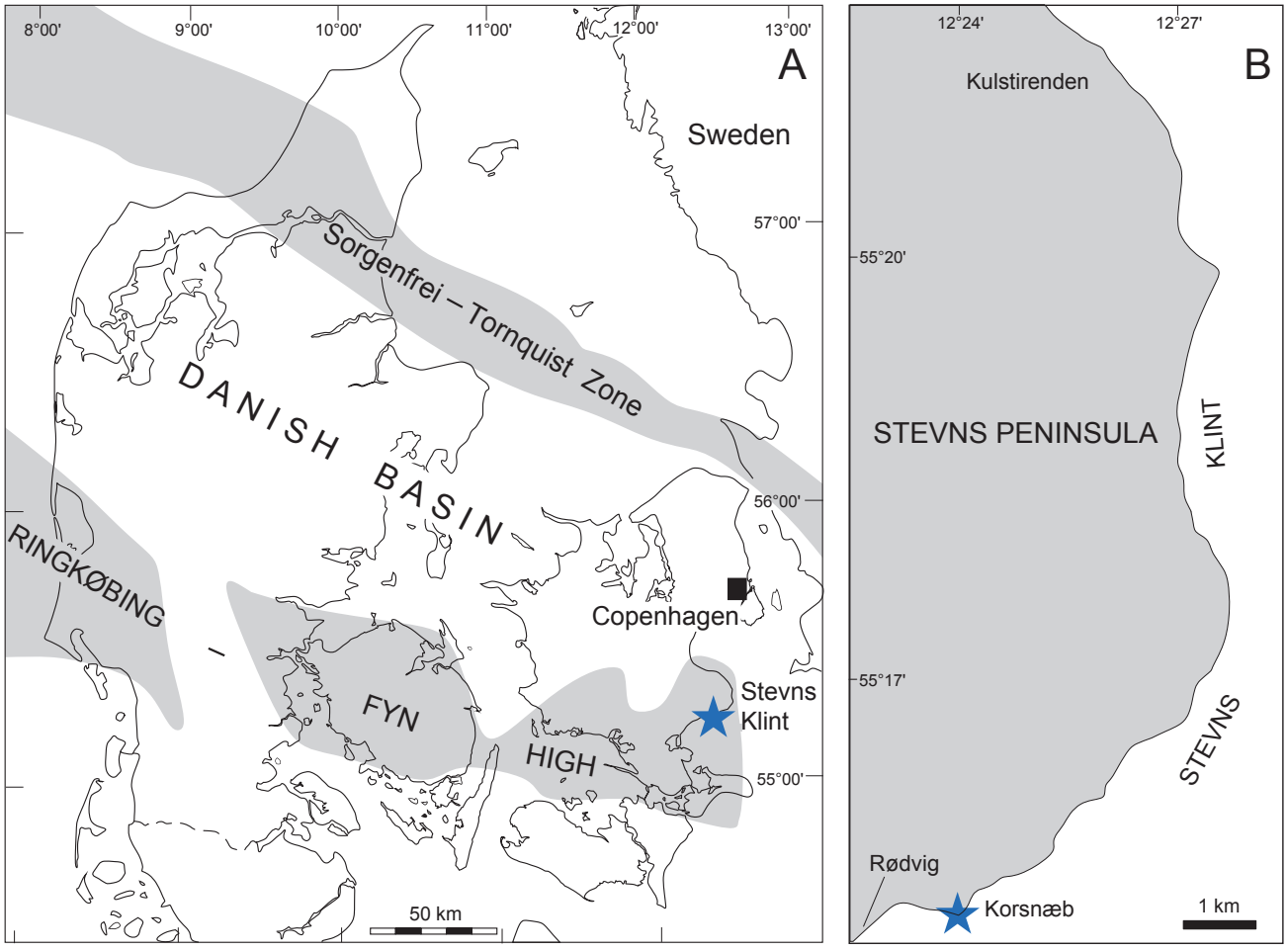

Fig. 2. A: Map of Denmark showing the major structural elements and the position of the studied section at Stevns Klint (blue star). **B**: Map of Stevns peninsula showing the location of the studied section at Korsnæb (55.25403°N, 12.39624°E), east of Rødvig. Modified from Rosenkrantz *et al.* (2021).

tian mounds of the Højerup Member and forms the base for the lower Danian bryozoan mounds of the Korsnæb Member (Stevns Klint Formation; Surlyk *et al.* 2006; Rosenkrantz. *et al.* 2021).

A wavy relief of the erosion surface suggests that the original sea-floor topography was formed by WNW-flowing bottom currents (Surlyk & Lykke-Andersen 2007). After erosion, the remaining Cerithium Limestone Member is preserved as a disjointed series of small depression fills, which are separated by truncated Maastrichtian mounds (Surlyk *et al.* 2006). The Cerithium Limestone Member shows thinning, condensation, or even erosion in the northern part of the Stevns Klint area (e.g., Surlyk *et al.* 2006). The depositional environment of the unit was marine and ranged from mid-neritic (30–100 m water depth) to a deeper milieu, as suggested by a high proportion of planktic foraminifera (e.g., Rasmussen *et al.* 2005; Surlyk *et al.* 2006).

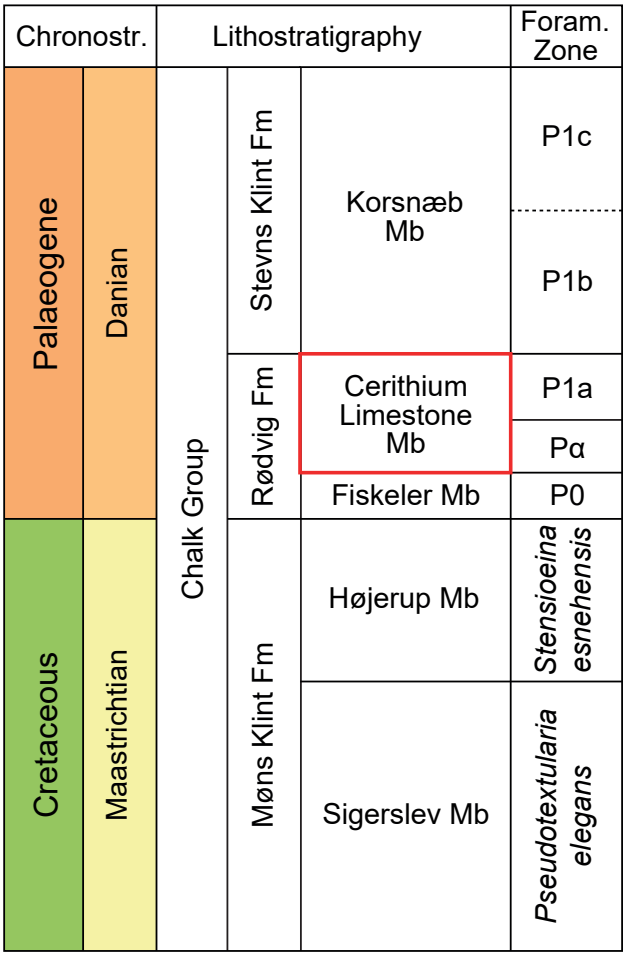

Fig. 3. Chronostratigraphy of the Cretaceous-Palaeogene interval along with the lithostratigraphy and the foraminiferal zonation at Stevns Klint. The Cerithium Limestone Member is indicated by a red rectangle (modified from Surlyk *et al.* 2006).

The Cerithium Limestone Member has been described both as fossil-poor, with only gastropods, echinoderms and crinoids (Rosenkrantz 1939), and as fossil-rich, with additional foraminifera (e.g., Schmitz *et al.* 1992; Hart *et al.* 2005; Rasmussen *et al.* 2005), bivalves (Heinberg 1999), siliceous sponges (Bernecker & Weidlich 2005), ammonites (Machalski & Heinberg 2005) and rare bryozoans (Heinberg 2005). Several species surviving the K–Pg event have been documented from the Cerithium Limestone Member, with the most remarkable discovery being several ammonites (Machalski & Heinberg 2005). Biostratigraphic studies have resulted in contrasting evidence and opinions concerning the age and duration of the Cerithium Limestone Member (Rasmussen *et al.* 2005).

Materials and methods

Two sampled profiles across the Cerithium Limestone Member at Rødvig were analysed. The initial profile is a 60 cm thick block that encompasses the entire vertical extent of the unit. To gain comprehensive insights into microfacies and the fossil content, twelve samples were selected for thin section production. The samples were chosen based on distinct characteristics of the limestone, such as burrows, colour changes or textural variations. Seventeen samples were prepared for scanning electron microscope (SEM) analyses, representing the various microfacies of the Cerithium Limestone Member. These samples were used to analyse the microfacies at the micro- and nanometre scales. Following the observation of diverse microfacies, seven additional samples were collected from a 60 cm vertical profile, with number 2 at the base until number 8 at the top of the section (Fig. 4). These samples were prepared for quantitative analyses of bioclast content and microfacies variability in the stratigraphic succession. From these seven samples, a total of fifteen thin sections were produced, with one per sample along the main vertical profile and duplicates for certain samples: two for sample 3, three for sample 4, one for sample 5 and two for sample 7.

During the thin section preparation, due to the brittle and soft nature of the Cerithium Limestone Member, the samples were embedded in epoxy, using a vacuum chamber to prevent any damage. Subsequently, the samples were manually ground and polished. Observations were conducted using an Olympus BX50 petrographic microscope equipped with a digital camera (Olympus SC50) and an electronic stepping stage for point counting, at the Department of Geology, Lund University. Lithologies

were classified according to the Dunham classification (Dunham 1962) and the modified scheme of Embry & Klovan (1971). Analyses of the microfacies (e.g., composition, fabrics and textures) were carried out according to Wilson (1975) and Flügel (2010).

The characteristics of the thin sections were quantified using Petrog 5 software. A random grid of points was selected, with the number of counts per thin section set at 250, as the threshold for statistical significance is considered to be at around 200 counts (Galehouse 1971). The bioclasts were classified at the order level, distinguishing between benthic and planktic foraminifera. Bioclasts were typically counted only if the pointer of the crosshair hit their shells, although complete shells were included in the count if the crosshair hit inside them. Variations in matrix colouration were divided into three groups: dark, intermediate and light matrix.

The samples for the SEM study were cut, polished and sputter-coated with platinum-palladium (Cressington sputter coater 108 auto, 20 mA, 20 seconds). The selection of seventeen samples was studied using a Tescan Mira3 High-Resolution Schottky field emission-scanning electron microscope equipped with an Oxford energy dispersive X-ray spectroscopy (EDS) at the Department of Geology, Lund University. Samples were imaged and analysed for microstructures related to sediment-influencing/-producing organisms and diagenetic processes. EDS was used for elemental analyses and to determine the chemical composition of the main components. Additionally, calcareous nannofossils were quantified along one

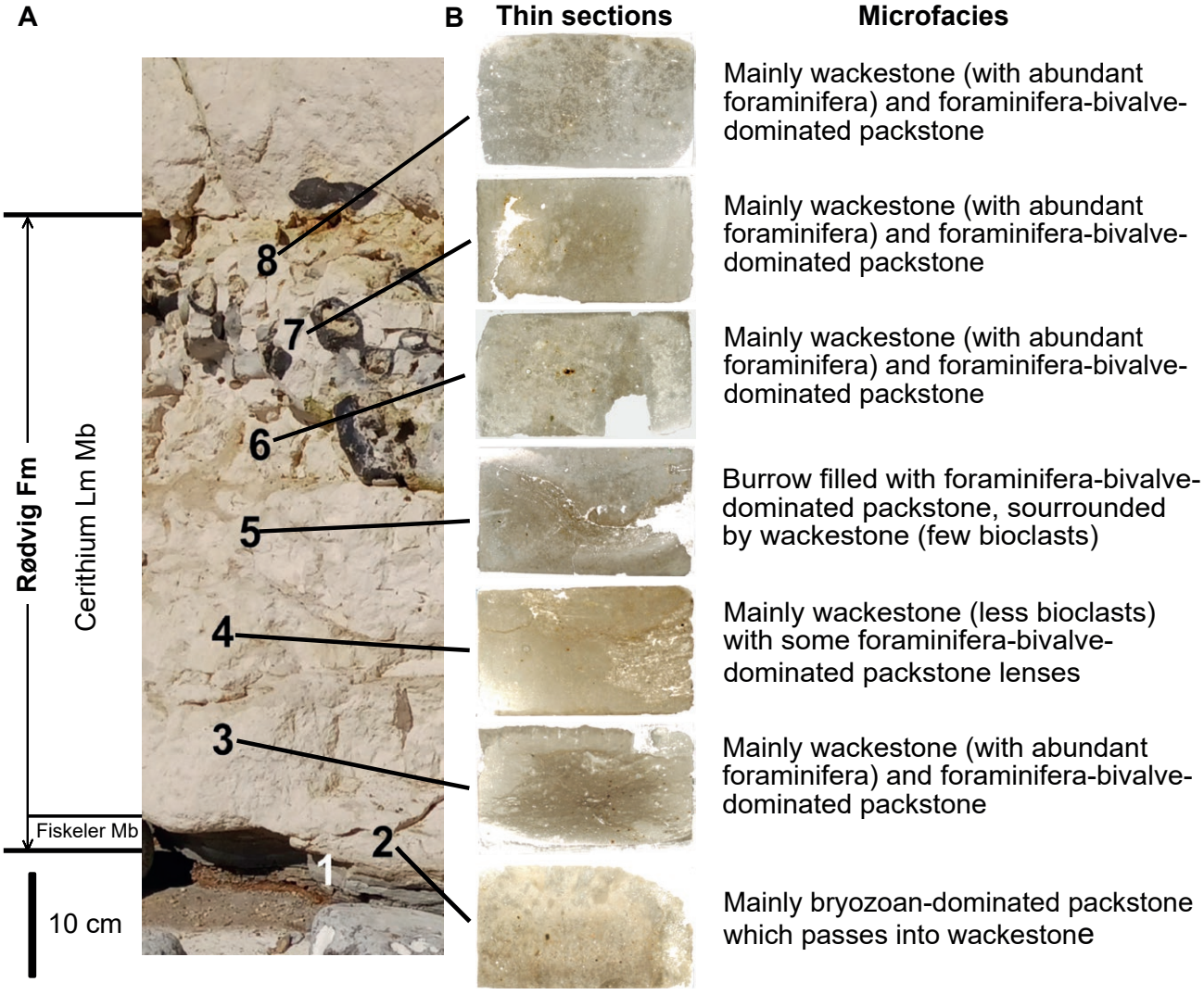

Fig. 4. Representation of the studied Rødvig section. **A**: Outcrop photograph of the K–Pg boundary strata east of Rødvig, indicating the sample levels. The Rødvig Formation includes the lowermost Danian Fiskeler Member, recording the iridium anomaly, and the overlying Cerithium Limestone Member studied in detail herein. **B**: Scanned images of seven thin sections from the vertical profile of the Cerithium Limestone in stratigraphic order with a description of their microfacies.

transect of ~1 cm in three samples: one at the base, one at the middle and one at the top of the section. All sample materials and thin sections are stored at the Department of Geology, Lund University, Sweden.

Results

The Cerithium Limestone Member in our section is ~ 0.6 m thick, beige-yellowish with an unevenly exposed surface (Figs 4, 5). The relatively soft lower part exhibits a beige colour, while the more cemented upper part appears pale yellow. At the macroscopic scale, the lithology appears homogeneous, with brown bioturbation tracks scattered throughout the section. Macrofossils occur locally and observed specimens include gastropods that are preserved as moulds.

Thin sections analyses – sedimentary microfacies

The position, overview image, microfacies and bioclast content of the thin sections along the vertical

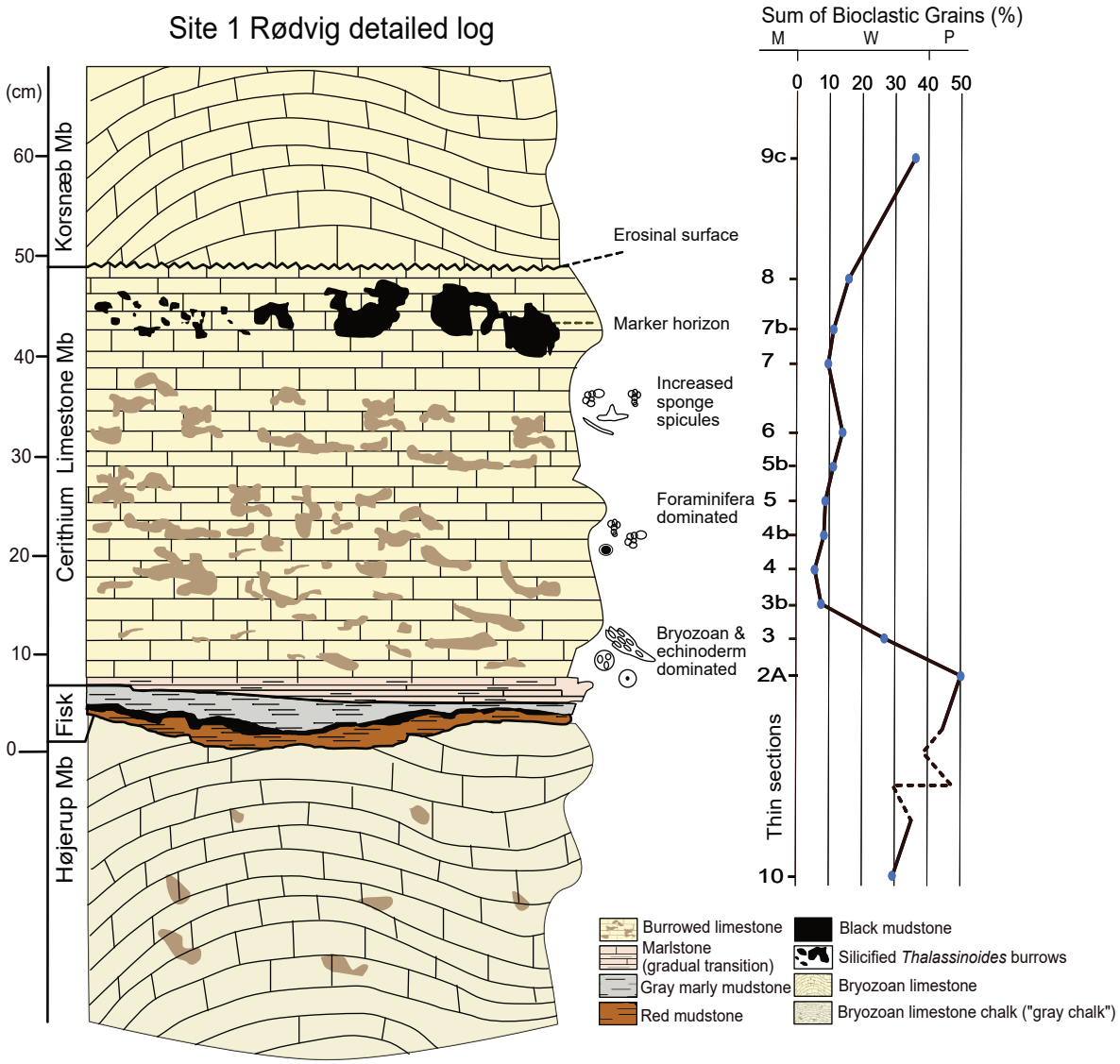

Fig. 5. Schematic representation of the Rødvig section, including the height, members and lithology, along with the total abundance of bioclasts in percentages. The different members of the sample site at Rødvig are on the left, Fisk: Fiskeler Member. Point counting results with bioclastic amounts are shown to the right of the log with the samples matched with the log's vertical scale. The percentage bioclastic amounts are grouped according to Dunham's classification with mudstone (M), wackestone (W) and packstone (P) respectively. The 0 in the section is the base of the Rødvig Formation, located approximately 1 m above sea level at the studied site. Highlights of the general fossil content from the samples are shown next to the log.

profile are summarised in Figs 4 and 5. Thin section analyses show that the Cerithium Limestone Member is composed of four distinct microfacies: a carbonate mudstone (Fig. 6A), a predominant wackestone (Fig. 6B), a foraminifera-bivalve-dominated packstone (Fig. 6C) and a bryozoan-dominated packstone (Fig. 6D).

Mudstone. The mudstone (Figs 6A1, A2) has less than 10% grains and is dominantly beige. The mud-sized matrix is mixed with few dark grey peloids, red iron oxides and yellowish pyrite. Recognisable fossils are scarce in this microfacies, with only a few bivalves, gastropods and foraminifera. Scattered benthic and planktic foraminifera are present with either the test preserved (Fig. 6A1) or just as a mould (Fig. 6A2). Most foraminifera tests or moulds are filled with black or brownish sediment. Small burrows are present within the mudstone and are filled with a foraminifera-bivalve-dominated packstone. The burrows are rich in bioclasts, including planktic and benthic foraminifera, ostracods, bivalves, gastropods, echinoderms and sponge spicules.

*Wackestone***.** The light grey wackestone contains iron-oxides and a larger number of pyrite and bioclasts compared to the mudstone (Fig. 6B1). In certain places, it contains large amounts of small dark grey peloids. Most fossils are planktic and benthic foraminifera, presenting a relatively broad range of sizes and species. Bivalves, ostracods, gastropods, echinoderms and bryozoans are also commonly observed. Calcareous dinoflagellates occur sparsely. The wackestone shows burrows with an infilling of a foraminifera-bivalve-dominated packstone (Figs 4B, 5). Abundant and relatively diverse bioclasts, with different sizes of planktic and benthic foraminifera, ostracods, bivalves, gastropods, echinoderms and sponge spicules, are identified in the burrows. Upon examination under a fluorescence light microscope, one of the burrows exhibits a white outline, indicating the presence of organic matter. Smaller burrows within the wackestone are filled with a fossil-rich packstone or wackestone. This packstone is rich in bioclasts including planktic and benthic foraminifera, ostracods, bivalves, gastropods, echinoderms and sponge spicules. Overall, the two described types of burrows show a high abundance of fossil assemblages, whereas a third type of burrows with a fine-grained mudstone infilling nearly lacks bioclasts as only a few scattered foraminifera are visible (Fig. 6E). These small-scale or micro-burrows with a diameter range <1 mm have multiple branching points and show in certain cases a connection to larger vertical shafts (Fig. 6E). They show an irregular margin and a branched distribution pattern in thin sections. They might represent thin *Chondrites* (Baucon *et al.* 2020). Note that due to significant differences in hardness and lithification, some parts of the fine-grained burrow infills were lost during the polishing of the thin sections (Fig. 4).

*Foraminifera-bivalve-dominated packstone***.** This packstone (Fig. 6C1) is dark brownish with a fine-grained matrix, iron oxides, pyrite, clay particles and peloids of different sizes. This microfacies is richer in bioclasts, including abundant and diverse planktic and benthic foraminifera, gastropods, bivalves, corals, ostracods, echinoderms and calcified sponge spicules. Bryozoans are scarce and skeletal grains often appear in clusters. The above-mentioned small-scale or micro-burrows with a fine-grained mudstone are also present in this packstone.

*Bryozoan-dominated packstone***.** This packstone (Fig. 6D) contains a large amount of bryozoan debris, broken mollusc shells, small foraminifera, calcite crystals, small oxides and small to large pyrites. The micrite has a beige colour with abundant, minute bioclastic debris and peloids. In certain areas, it could be referred to as a wackestone. No burrows were seen in this microfacies. The bryozoan-dominated packstone is only present in sample 2 (Figs 4, 5, 6D), just above the Fiskeler Member. The transition to the dominating wackestone microfacies is observed in sample 3.

Vertical stratigraphic development

Along the vertical profile, the first 7–12 cm above the Fiskeler Member are mainly composed of the bryozoan-rich packstone (sample 2; Figs. 4, 5, 6D). Above this, a progressive transition over several centimetres into the dominant wackestone microfacies is visible, marked by the disappearance of bryozoan components. Throughout the Cerithium Limestone Member, foraminifera-bivalve-dominated packstone forms isolated concentrations, mostly associated with burrowing activity. The mudstone microfacies is frequently observed in small fractures and burrows (Fig. 6E).

Except for the lowermost bryozoan-dominated layer, the most abundant fossils in the Cerithium Limestone Member (under light microscope) are planktic and benthic foraminifera, with a predominance of the latter. Transitions between microfacies are either sharp, especially between burrows and the surrounding rock, or gradual, with a progressive increase in the number of bioclasts.

Bioclast abundance

The point counting results (Fig 5, supplementary material, Table S1) indicate the highest abundance of bioclasts, reaching up to 50% of bioclastic grains, in

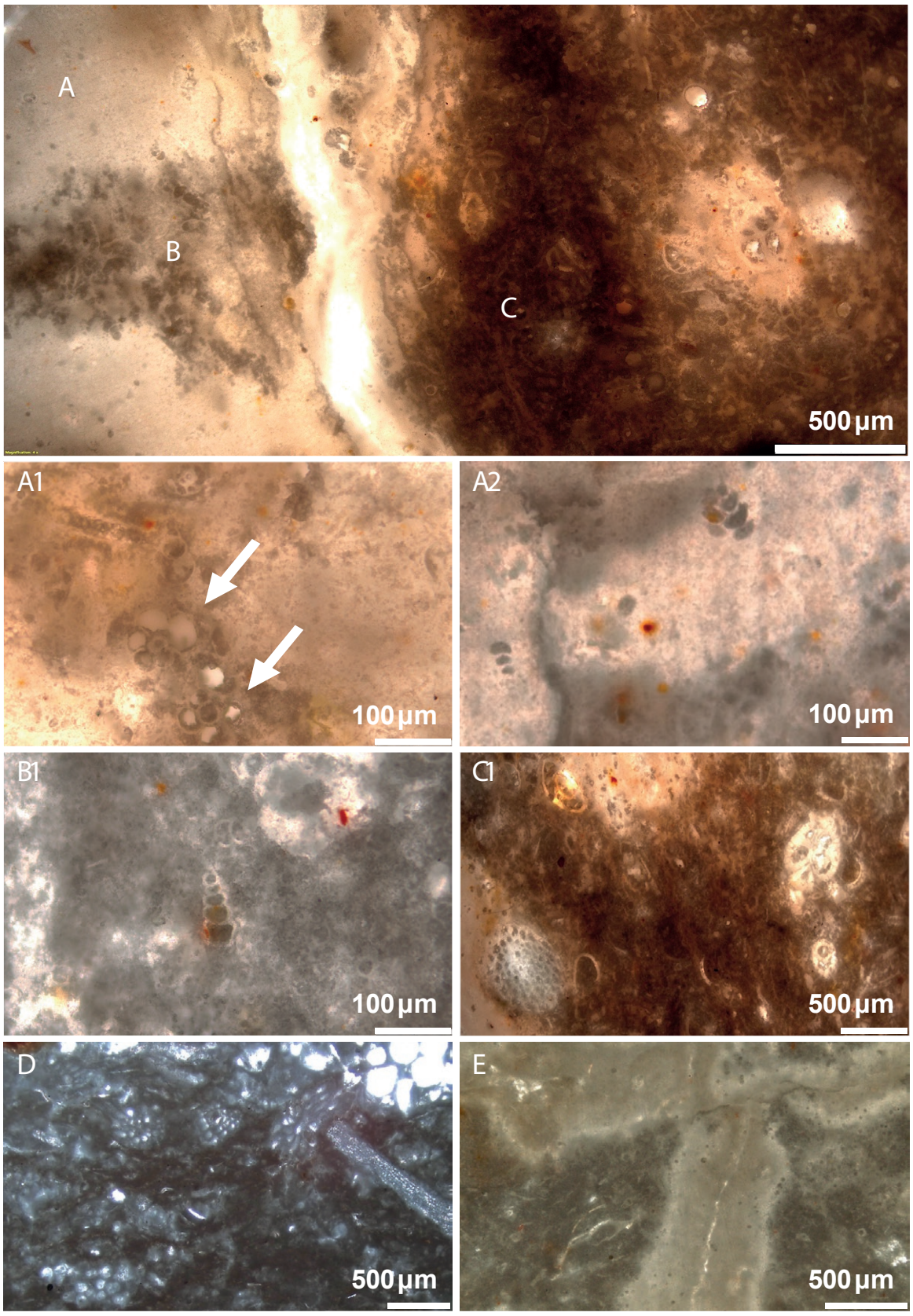

Fig. 6. Optical microscope images of thin sections from the Cerithium Limestone show four different microfacies with A: mudstone, B: wackestone, C: foraminifera-bivalve-dominated packstone and D: bryozoan-dominated packstone. **A1,2**: Mudstone including preserved foraminifera test (A1) and filled moulds of foraminifera (A2). **B1**: Wackestone with foraminifera. **C1**: Foraminifera-bivalve-dominated packstone with abundant fossil content. **D**: Bryozoan-dominated packstone with abundant bryozoans. **E**: A burrow in wackestone filled with mudstone.

the basal sample 2 corresponding to the bryozoan-rich packstone microfacies. The grain abundance gradually decreases to around 10% in the main part of the Cerithium Limestone Member through samples 3 to 7. The uppermost part of the Cerithium Limestone Member is characterised by an increase in abundance with around 15% bioclastic grains, mainly calcified sponge spicules and rare bryozoans.

SEM analyses

Microfacies analyses under SEM

Under the SEM, the mudstone and wackestone exhibit the highest porosity (Figs 7, 8). The freshly cut and polished samples show deep and elongated holes in the matrix. Cementation occurs sparsely in those two microfacies and consists of low-Mg-calcite crystals without silica, as indicated by elemental mapping. The matrix of the wackestone and mudstone microfacies is composed of small crystalline calcite with a dominance of 1–4 μm crystals (Fig. 7). Very small, equant crystals below 1 μm in size occur in clusters and crystals up to 10 μm are also present. Calcite spar crystals of up to 15 μm were occasionally observed. In general, the shape of the crystals shows a variety of polyhedral forms with reduced corners but edges visible. Dissolution attributed to early diagenetic alterations is apparent on both the matrix and crystals in all microfacies (Fig. 7 A, B). Observations reveal cracks and dissolution pits, along with crystals with reduced corners and edges, leading to the transformation of rhombohedral shapes into polyhedral forms (Fig. 7 A, B).

Changes in microfacies are either gradual (Fig. 8A), with a progressive increase in the number of bioclasts, or sharp, especially between burrows and the surrounding rock. In the wackestone, bioclasts are loosely packed, with few in close contact with each other (Fig. 8B). Sharp boundaries are most commonly found in the transition zone from the mudstone to the foraminifera-bivalve-dominated packstone (Fig. 8F). A change from the mudstone and wackestone to the foraminifera-bivalve-dominated packstone is clearly visible through a significant increase in bioclasts (Figs 8A, C, F). Densely packed bioclasts are present in both packstone varieties (Figs 6C1, D, 8D, E). The packstones

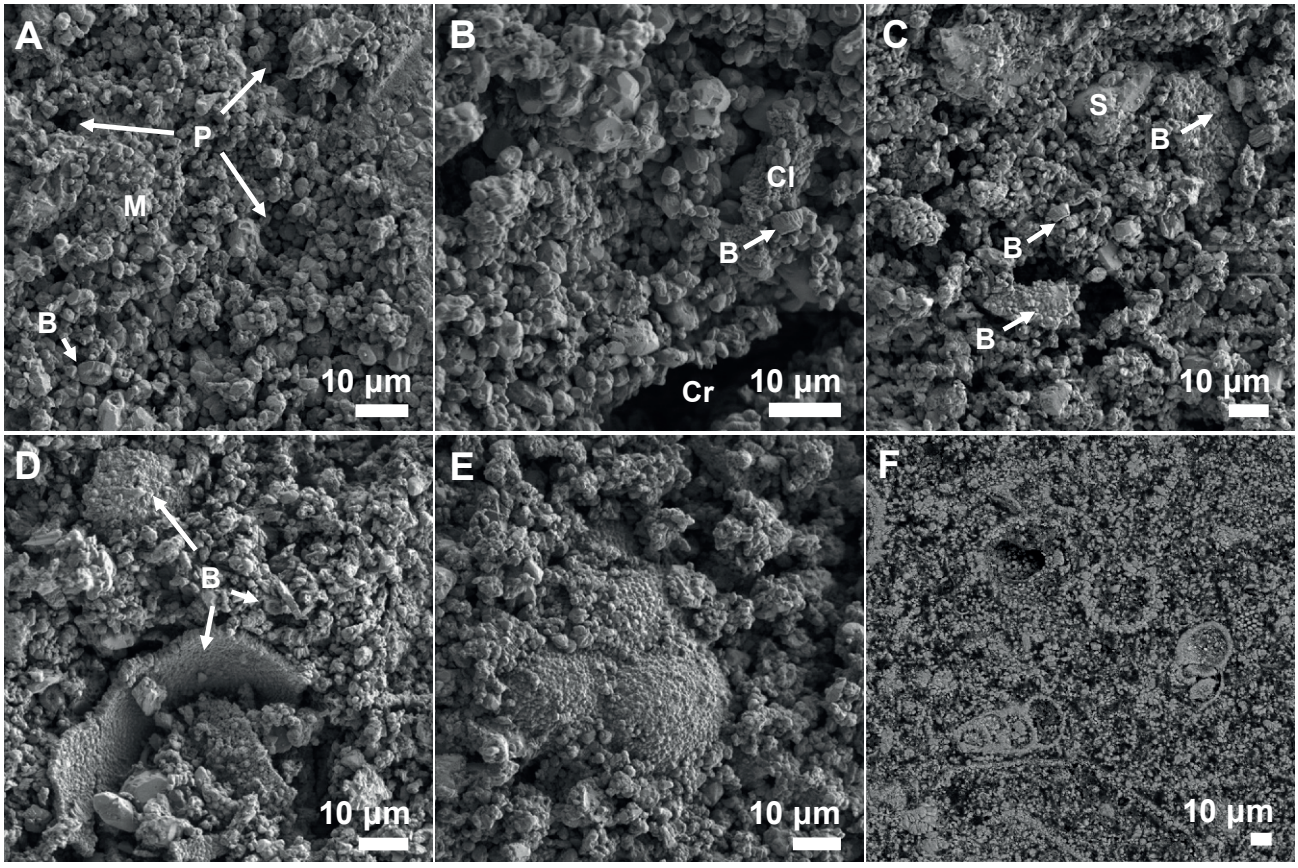

Fig. 7. Scanning electron microscopy images of the four different microfacies in the Cerithium Limestone. **A**: Mudstone. **B**: Wackestone with cracks and clusters. **C**: Foraminifera-bivalve-dominated packstone with bioclasts and spar. **D**: Foraminifera-bivalve-dominated packstone with bioclasts. **E**: Foraminifera covered in fine microcrystals in the wackestone. **F**: Bryozoan-dominated packstone, B: bioclasts, Cl: cluster, Cr: crack, M: micrite, P: porosity, S: spar.

are less porous than the other two microfacies (Figs 7C, D, F). Deep and elongated cracks are absent, and crystals have more contact surfaces in between. The size and shape of the calcite crystals are highly variable, with increasingly larger crystals including some exceeding 15 μm (Fig. 7C). However, as for the other microfacies, micrite with crystals smaller than 4 μm is dominant. Most crystals show a rough surface with many cracks. Cement is present in the foraminifera-bivalve-dominated packstone and consists of low Mg-calcite and no silica, as indicated by element mapping (see supplement Fig. S1).

Microfossil analyses under SEM

Studies of the microfossil content under the SEM show a few scattered foraminifera and calcareous nannofossils in the mudstone, while the wackestone shows more abundant fossils (Figs. 7B, E, 8B, D). Foraminifera were observed as fragments or complete with either the tests preserved covered by calcite microcrystals (Fig. 7E) or as imprints (Fig. 8B). Additionally, numerous calcareous nannofossils (Fig. 7D) with mainly coccoliths and few calcareous dinoflagellate cysts (see supplement Pl. S1) were observed in all microfacies with different abundances. Sample 2, at the base of the section, shows the poorest preservation and records the lowest abundance of calcareous nannofossils with ~ 8×10^2 nannofossils/cm^2 (Table S2). Sample 4 exhibits very good preservation with entire coccospheres and coccoliths preserved. This sample presents the highest abundance of calcareous nannofossils with ~ 1×10^4 nannofossils/cm^2 (Table S2). Sample 8, at the top of the section, exposes fewer calcareous nannofossils with ~ 3×10^3 nannofossils/cm^2 (Table S2). The coccolith assemblage comprises 10–15 (Pl. S1) species with a dominance of *Arkhangelskiella cymbiformis* (Vekshina 1959), *Biscutum castrorum* (Black & Barnes 1959), *Biscutum harrisonii* (Varol 1989), *Neocrepidolithus neocrassus* (Perch-Nielsen 1968; Romein 1979) and *Neocrepidolithus* spp. Rare *Ahmuellerella regularis* (Górka

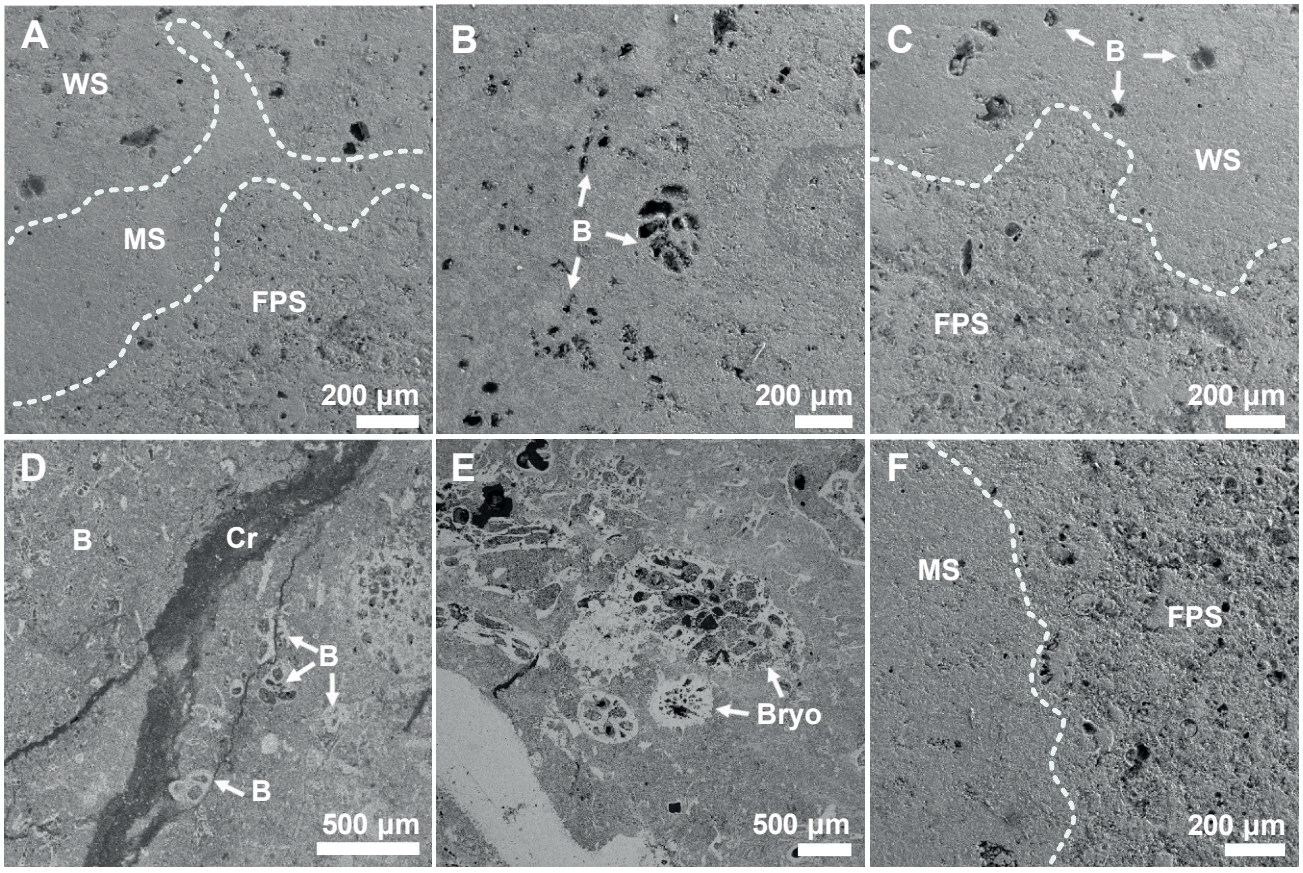

Fig. 8. Scanning electron microscopy images of thin sections from the Cerithium Limestone. **A**: Three microfacies of the upper part of the limestone with their boundaries illustrated in dashed lines. **B**: Wackestone with bioclasts including imprints of dissolved tests of foraminifera. **C**: Transition from wackestone to the foraminifera-bivalve-dominated packstone. **D**: Foraminifera-bivalve-dominated packstone with a high amount of preserved tests of foraminifera. **E**: Bryozoan-dominated packstone with bryozoans. **F**: Transition zone from foraminifera-bivalve-dominated packstone to mudstone. B: bioclasts, Bryo: bryozoans, Cr: crack, FPS: foraminifera-bivalve-dominated packstone, MS: mudstone, WS: wackestone. The white dashed line shows the transition between the microfacies.

1957; Reinhardt & Górka 1967), *Kamptnerius magnificus* (Deflandre 1959), *Nephrolithus frequens frequens* (Górka 1957), *Watznaueria fossacincta* (Black 1971; Bown & Cooper 1989), *Zeugrhabdotus sigmoides* (Bramlette & Martini 1964; Bown & Young 1997), *Markalius apertus* (Perch-Nielsen 1979), *Markalius inversus* (Deflandre & Fert 1954; Bramlette & Martini 1964), *Prediscosphaera stoveri* (Perch-Nielsen 1968; Shafik & Stradner 1971) and *Cyclagelosphaera alta* (Perch-Nielsen 1979) were observed. Calcareous dinoflagellates are mostly preserved as half-broken but well-preserved specimens of *Cervisiella operculata* (Bramlette & Martini 1964; Streng *et al.* 2004) with a size of up to 20 μm (Pl. S1).

Different fragments of bioclasts such as fish teeth, broken shells of macrofossils, bryozoans and microfossils were observed, with the highest amount in the packstone microfacies.

Discussion

Fossil content

The Cerithium Limestone Member is described as a fossil-rich unit with gastropods, echinoderms, crinoids, foraminifera, bivalves, calcified siliceous sponges, ammonites and occasionally bryozoans (e.g., Machalski & Heinberg 2005; Rasmussen *et al.* 2005). In our thin section analyses, we find two different parts within the Cerithium Limestone Member that may have stratigraphic significance. The lowermost part, in contact with the Fiskeler Member, consists of a bryozoan-dominated packstone with bivalves, foraminifera and gastropods (Figs 4, 5, 6D, 8E). This bryozoan-dominated packstone does not re-appear higher up in the Cerithium Limestone Member. The high amount of bryozoans and broken bioclasts, the presence of calcite crystals, and the low amount of micrite compared to the rest of the Cerithium Limestone Member, suggest reworking of older sediments. These may have originated from the crest of the Maastrichtian mounds surrounding the depression where the Cerithium Limestone Member has been preserved (Surlyk *et al.* 2006).

The upper, main part of the Cerithium Limestone Member is dominated by the wackestone microfacies with foraminifera, bivalves, gastropods, echinoderms, crinoids, calcified siliceous sponges and rare bryozoans. Despite poor preservation, Rasmussen *et al.* (2005) reported an abundant but low-diversity assemblage of foraminifera in the 40–125 μm fraction from the Cerithium Limestone Member. Standard foraminiferal biostratigraphy from different studies (e.g., Heinberg 2005; Rasmussen *et al.* 2005) indicates that the Cerithium Limestone Member belongs to the Pα and the P1a zones (Fig. 3). The section at Rødvig represents mainly the Pα foraminiferal zone and was possibly deposited within 400 ka (Heinberg 2005; Rasmussen *et al.* 2005; Ogg *et al.* 2016), with both the Pα and the P1a zones representing less than 800 ka (Ogg *et al.* 2016). These findings suggest that the wackestone was deposited during an initial stage of the post-extinction recovery interval during the earliest Danian, rather than being a result of reworking of older sediments.

Fossils have also been impacted by dissolution, as indicated by the visible internal and external moulds of test fragments of foraminifera, resulting from the dissolution of the original tests (Fig. 6A2). The random occurrence of those foraminifera moulds, both horizontally and vertically, suggests widespread dissolution affecting the entire section. Species-specific resistance or weakness to dissolution seems unlikely as both benthic and planktic species were affected. Imprints in the sediment suggest that the dissolution of the tests occurred after the lithification of the host rock. Poor preservation and issues such as dissolution and fragmentation of foraminifera have been reported previously (Hart *et al.* 2005; Rasmussen *et al.* 2005). Any (re-)evaluation of foraminiferal zonation along the cliff exposure should take into account the very local changes in the type of preservation of the foraminifera, which evidently can vary within a few centimetres.

The SEM observations revealed the presence of calcareous nannofossils, including dinoflagellate cysts in low abundance and coccoliths in higher abundance in all microfacies (Fig. 7). In contrast to the foraminifera, dissolution was not apparent in the calcareous nannofossils, which occur with good preservation; even coccospheres are preserved. Only the calcareous nannofossils in sample 2, just above the K–Pg extinction interval, show slight dissolution features. Quantification indicates an abundance of calcareous nannofossils ranging between 8×10^2 and 1×10^4 nannofossils/cm^2. Just prior to the K–Pg mass extinction, the latest Cretaceous recorded the highest abundance and diversity of calcareous nannofossils of the entire Mesozoic Era, with up to 149 recognised species and a yearly deposition on the order of 10^7 nannofossils/cm^2 (Bown *et al.* 2004; Suchéras-Marx *et al.* 2019). The low abundance and diversity (10–15 species) of calcareous nannofossils in the Cerithium Limestone Member attest to the K–Pg mass extinction event affecting calcifying nannoplankton.

Among the calcareous dinoflagellate cysts, *Cervisiella operculata* (Pl. S1) dominates the assemblage but does not occur in high abundance. *C. operculata* is abundant in low-latitude successions (Guerra *et al.* 2021) and is used as a marker for the earliest Danian

(McLachlan & Pospelova 2021). This species is described as a 'disaster taxon', flourishing in stressed environmental conditions (Wendler & Willems 2002; Hildebrand-Habel & Streng 2003; Bralower *et al*. 2020; Guerra *et al*. 2021; Mahanipour *et al*. 2022) due to reduced competition (Guerra *et al*. 2021) and the sudden appearance of vacant niches (Smit 2005). *C. operculata* is suggested to indicate warm water environments (Egger *et al*. 2009; Mohamed *et al*. 2012) and decreased primary productivity (Guerra *et al*. 2021).

In our samples, coccoliths were found in higher abundance than the calcareous dinoflagellate cysts. Using the terminology of Bernaola & Monechi (2007), the assemblage contains a few Cretaceous-vanishing (C-vanishing) species, such as *A. cymbiformis, A. regularis, K. magnificus, N. frequens frequens, P. stoveri* and *W. fossacincta*. The C-vanishing species include all Cretaceous species that became extinct at or below the boundary and species that progressively disappeared in the lowest metres of the Danian (Bernaola & Monechi 2007). The evolution of the calcareous nannoplankton across the K–Pg transition is not fully understood, but most studies explain the presence of the rare C-vanishing species by reworking (e.g., Bown 2005; Minoletti *et al*. 2005).

The Cretaceous-persistent (C-persistent) species are, on the contrary, considered survivors from the Mesozoic into the Cenozoic era (Bernaola & Monechi 2007). C-persistent species include Cretaceous species found in low abundance in the uppermost Maastrichtian but persist well into the Palaeogene, where their relative abundance increases (Bernaola & Monechi 2007). In our samples, C-persistent species are represented by *Biscutum* spp., *Markalius* spp., *Neocrepidolithus* spp., *Z. sigmoides* and *C. operculata*. They are relatively more abundant than the C-vanishing species, but our quantification results show a low total abundance, arguing in favour of the persistence of harsh environmental conditions during the deposition of the Cerithium Limestone Member. Finally, the presence of *C. alta* in sample 4 marks the appearance of a new Paleocene taxon.

Origin of the micrite

In the aftermath of the K–Pg event, oceanic productivity recovered rapidly in terms of biomass (Alegret *et al*. 2012) with hypothetical eutrophication supporting the plankton blooms (Alegret *et al*. 2012). Global post-impact 'whitings' caused by cyanobacterial blooms may have contributed to the formation of the pale grey marly chalk of the Fiskeler Member, directly underlying the Cerithium Limestone Member (Bralower *et al*. 2020). In certain localities, these global whiting events might have persisted for thousands of years after the K–Pg event (Bralower *et al*. 2020) and continued until the deposition of the Cerithium Limestone Member. Cyanobacterial blooms in whitings require $CaCO_3$ supersaturation in seawater (Jones *et al*. 2019). The abrupt extinction of calcifiers (Bown 2005) and a lowered $CaCO_3$-to-organic carbon rain ratio (Henehan *et al*. 2016) possibly resulted in supersaturated surface waters (Bralower *et al*. 2020).

The presence of cyanobacteria in the Fiskeler Member at Stevns Klint has been inferred on the basis of organic biomarkers for bacterial productivity (Sepulveda *et al*. 2009; Schaefer *et al*. 2020). A high abundance of steranes and hopanes (in the Fiskeler Member) reflects a rapid recovery (*c.* 10^2–10^3 years) of bacterial and algal production in the area (Sepúlveda *et al*. 2009), suggesting thriving cyanobacterial communities (Schaefer *et al*. 2020). The survival of cyanobacteria without significant losses in the extinction event (Sepulveda *et al*. 2009; Alegret *et al*. 2012) and their possibly unique adaptation to the extreme post-extinction environments may have contributed to micrite precipitation (Robbins & Blackwelder 1992; Thompson 2000; Obst *et al*. 2009; Bralower *et al*. 2020).

Although different microfacies occur in the Cerithium Limestone Member, the rock matrix is consistently dominated by small calcite crystals in the micron size range (< 4 μm; Fig. 7). In this respect, our observations confirm those of Hansen (1990). Hansen (1990) defined the rock unit as extremely loose, with no or little attachment between crystals and with a richness of small grains ranging between 1 and 5 μm in size. The dominance of calcite crystals smaller than 4 μm in size, with rare or absent microbioclast debris, suggests a microbial origin of the Cerithium Limestone Member, possibly from cyanobacteria (Flügel 2010). Moreover, EDS analyses of the four microfacies indicate a low-Mg-calcite composition, as also reported by Hansen (2019). Low-Mg calcite with microcrystals in the 1–9 μm size range is globally characteristic of Phanerozoic limestones (Kaczmarek *et al*. 2015) and is typical of cyanobacterial whiting (Bralower *et al*. 2020). Thus, we suggest that the micrite of the Cerithium Limestone Member was formed due to the high abundance of cyanobacteria. Abundant cyanobacteria would entail strong photosynthetic activity, leading to an increase in alkalinity that ultimately triggered whiting events, enabling the precipitation of micrite.

Microfacies types and environmental conditions

Our study reveals that the Cerithium Limestone Member mainly consists of two relatively distinct stratigraphic parts: the first is the lowermost part of the unit and likely constitutes a thin layer of Maastrichtian reworked material. The second and major part is a burrowed limestone comprising mudstone,

wackestone and foraminifera-bivalve-dominated packstone microfacies. These microfacies types are typical for open marine, mid–outer carbonate ramps/shelves (Flügel 2010). The bioclastic wackestone and packstone with diverse, common to abundant fossils and peloids (which occur as mudstone peloids in outer ramps), are characteristic of the outer ramp microfacies type RMF 3 (Flügel 2010). Notably, the microfacies occur randomly; in the vertical profile (Fig. 4), above sample 3, all three microfacies occur in each sample and no distributional pattern or depositional succession of the microfacies is discernible. An explanation for the random distribution of the microfacies might be a high degree of bioturbation as exemplified by *Thalassinoides*, *Spongeliomorpha*-type burrows (Ekdale & Bromley 1984) and other ichnofossils (Rasmussen 1971). The bioturbation can be partly described as endichinal (common) and exichnial (from above) with the toponymic classification system after Martinsson (1970). Burrows typically occur across the ramp but are particularly abundant below the wave base and storm wave base (Flügel 2010).

Deposition of the Cerithium Limestone Member in cooler, deeper waters was suggested by the finding of shark teeth belonging to species living in deeper waters (Adolfssen & Ward 2015). These conditions confirm the interpretation of an open marine, outer ramp setting for the deposition of the Cerithium Limestone Member as suggested by our detailed microfacies analyses. The deposition and accumulation of carbonate mud clouds from the water surface implies generally low-energy conditions in a calm marine area. However, it is plausible that seasonal and relatively strong winds or storm events resulted in periodic bottom currents (Bjerager & Surlyk 2007) and facilitated the transportation of fossils, which accumulated in previously formed burrows. In summary, we suggest that the Cerithium Limestone Member was deposited in an open marine, outer-ramp-like setting in a dominantly low-energy environment.

Conclusions

This study reports detailed descriptions of thin sections of the Cerithium Limestone Member (Rødvig Formation) at Stevns Klint, Denmark. Four main microfacies were identified during microscopic investigations: a carbonate mudstone, a wackestone and two types of packstones. Our study confirms that the Cerithium Limestone Member is composed of two stratigraphically distinct parts, as previously assumed. The lowermost part consists of a thin layer of a bryozoan-rich packstone, interpreted as reworked material from the crests of the underlying Maastrichtian mounds. The second major part of the rock unit is an intensely burrowed limestone consisting of wackestone with predominantly foraminifera, mudstone with few foraminifera and foraminifera-bivalve-dominated packstone microfacies. A random spatial distribution of the microfacies suggests a high degree of bioturbation, as indicated by a variety of burrows. It is possible that the Cerithium Limestone Member had previously shown some stratigraphic development in its (micro-)facies characteristics, but this was erased due to bioturbation. SEM and light microscopy observations enabled the identification of various fossils, including planktic and benthic foraminifera, gastropods, bivalves, corals, ostracods, echinoderms, calcified sponge spicules and nannofossils. The predominance of small calcite crystals (1–4 μm) and the general shape of these crystals indicate that a significant portion of the micrite might have been formed through precipitation driven by microbial activity. The Cerithium Limestone Member is interpreted as formed in a mainly low-energy, open-marine, outer ramp-like sedimentary environment. In conclusion, the thin sections of the Cerithium Limestone Member at Stevns Klint provided new insights into the genesis of this famous rock unit.

Acknowledgements

This research received funding from the European Research Council (ERC) under the European Union's Horizon 2020 Research and Innovation Programme (Grant agreement No. 833454) and by a grant from the Knut and Alice Wallenberg Foundation to Daniel J. Conley. Anders Lindskog acknowledges funding from the Birgit and Hellmuth Hertz' Foundation and the Royal Physiographic Society in Lund. We received a sample permit for this protected area from the Geo-Museum Faxe, thanks to Jesper Milàn. We thank Carl Alwmark and Josefin Martell for their help with the SEM. Constructive reviews by Morten Bjerager and Finn Surlyk are gratefully acknowledged.

References

Adolfssen, J.S. & Ward, D.J. 2015: Neoselachians from the Danian (early Paleocene) of Denmark. Acta Palaeontologica Polonica 60, 313–338. https://doi.org/10.14202/app.2012.0123

Alegret, L., Thomas, E. & Lohmann, K.C. 2012: End-Cretaceous marine mass extinction not caused by productivity collapse. Proceedings of the National Academy of Sciences

of the United States of America 109, 728–732. https://doi.org/10.1073/pnas.1110601109

Alvarez, L.W., Alvarez, W., Asaro, F. & Michel, H.V. 1980: Extraterrestrial cause for the cretaceous-tertiary extinction. Science 208, 1095–1108. https://doi.org/10.1126/science.208.4448.1095

Alvarez, S.A., Gibbs, S.J., Bown, P.R., Kim, H., Sheward, R.M. & Ridgwell, A. 2019: Diversity decoupled from ecosystem function and resilience during mass extinction recovery. Nature 574, 242–245. https://doi.org/10.1038/s41586-019-1590-8

Baucon, A. *et al*. 2020: Ethology of the trace fossil Chondrites: Form, function and environment. Earth-Science Reviews 202, 102989. https://doi.org/10.1016/j.earscirev.2019.102989

Bernaola, G. & Monechi, S. 2007: Calcareous nannofossil extinction and survivorship across the Cretaceous-Paleogene boundary at Walvis Ridge (ODP Hole 1262C, South Atlantic Ocean). Palaeogeography, Palaeoclimatology, Palaeoecology 255, 132–156. https://doi.org/10.1016/j.palaeo.2007.02.045

Bernecker, M. & Weidlich, O. 2005: Azooxanthellate corals in the Late Maastrichtian Early Paleocene of the Danish basin: bryozoan and coral mounds in a boreal shelf setting. In: Bernecker, M. & Weidlich, O. (eds): Cold-water corals and ecosystems, 3–25. Berlin: Springer. https://doi.org/10.1007/3-540-27673-4_1

Birch, H.S., Coxall, H.K., Pearson, P.N., Kroon, D. & Schmidt, D.N. 2016: Partial collapse of the marine carbon pump after the Cretaceous-Paleogene boundary. Geology 44, 287–290. https://doi.org/10.1130/G37581.1

Bjerager, M. & Surlyk, F. 2007: Benthic palaeoecology of Danian deep-shelf bryozoan mounds in the Danish Basin. Palaeogeography, Palaeoclimatology, Palaeoecology 250, 184–215. https://doi.org/10.1016/j.palaeo.2007.03.008

Black, M. 1971: Coccoliths of the Speeton Clay and Sutterby Marl. Proceedings of the Yorkshire Geological Society 38, 381–424. https://doi.org/10.1144/pygs.38.3.381

Black, M. & Barnes, B. 1959: The structure of coccoliths from the English chalk. Geological Magazine 96, 321–328. https://doi.org/10.1017/S0016756800062294

Bown, P. 2005: Selective calcareous nannoplankton survivorship at the Cretaceous-Tertiary boundary. Geology 33, 653–656. doi:10.1130/G21566.1

Bown, P.R. & Cooper, M.K. E. 1989: New calcareous nannofossils from the Jurassic. Journal of Micropalaeontology 8, 91–96. https://doi.org/10.1144/jm.8.1.91

Bown, P.R. & Young, J.R. 1997: Mesozoic calcareous nannoplankton classification. Journal of Nannoplankton Research 19, 21–36. https://doi.org/10.58998/jnr2027

Bown, P.R., Lees, J.A. & Young, J.R. 2004: Calcareous nannoplankton evolution and diversity through time. In: Thierstein, H.R. & Young, J.R. (eds): Coccolithophores: from molecular processes to global impact, 481–508. Berlin: Springer. https://doi.org/10.1007/978-3-662-06278-4_18

Bralower, T.J. *et al*. 2020: Origin of a global carbonate layer deposited in the aftermath of the Cretaceous-Paleogene boundary impact. Earth and Planetary Science Letters 548, 116476. https://doi.org/10.1016/j.epsl.2020.116476

Bramlette, M.N. & Martini, E. 1964: The great change in calcareous nannoplankton fossils between the Mastrichtian and Danian. Micropaleontology 10, 291–322. https://doi.org/10.2307/1484577

Chenet, A.L., Courtillot, V., Fluteau, F., Gerard, M., Quidelleur, X., Khadri, S.F.R., Subbarao, K.V. & Thordarson, T. 2009: Determination of rapid Deccan eruptions across the Cretaceous-Tertiary boundary using paleomagnetic secular variation: 2. Constraints from analysis of eight new sections and synthesis for a 3500-m-thick composite section. Journal of Geophysical Research-Solid Earth 114, B06103. https://doi.org/10.1029/2008JB005644

D'Hondt, S. 2005: Consequences of the cretaceous/paleogene mass extinction for marine ecosystems. Annual Review of Ecology Evolution and Systematics 36, 295–317. https://doi.org/10.1146/annurev.ecolsys.35.021103.105715

Deflandre, G. 1959: Sur les nannofossiles calcaires et leur systématique. Revue de Micropaléontologie 2, 127–152.

Deflandre, G. & Fert, C. 1954: Observations sur les coccolithophoridés actuels et fossiles en microscopie ordinaire et électronique. Annales de Paléontologie 40, 115–176.

Dunham, R.J. 1962: Classification of carbonate rocks according to depositional texture. In: Ham, W.E. (ed.): Classification of carbonate rocks – A symposium. American Association of Petroleum Geologists Memoir 1, 108–121. https://doi.org/10.1306/M1357

Egger, H., Koeberl, C., Wagreich, M. & Stradner, H. 2009: The Cretaceous-Paleogene (K/Pg) boundary at Gams, Austria: Nannoplankton stratigraphy and geochemistry of a bathyal northwestern Tethyan setting. Stratigraphy 6, 333–347. https://doi.org/10.29041/strat.06.4.04

Ekdale, A.A. & Bromley, R.G. 1984: Sedimentology and ichnology of the Cretaceous-Tertiary boundary in Denmark – implications for the causes of the terminal Cretaceous extinction. Journal of Sedimentary Petrology 54, 681–703. https://doi.org/10.1306/212F84D6-2B24-11D7-8648000102C1865D

Embry, A. & Klovan, J. 1971: A late Devonian reef tract on northeastern Banks Island, N.W.T. Bulletin of Canadian Petroleum Geology 19, 730–781.

Flügel, E. 2010: Microfacies of carbonate rocks, 2nd edition, 976 pp. Berlin: Springer. https://doi.org/10.1007/978-3-642-03796-2

Forchhammer, G. 1825: De geognostostiske forhold i en Deel af Sjelland og Naboeöerne. Det Kongelige Danske Videnskabers Selskab, physiske og mathematiske Skrifter 1, 248–280.

Frederiksen, A., Thibault, N., Gilleaudeau, G.J., Bjerrum, C.J., Moreau, J. & Frei, R. 2024: Combined cadmium and chromium isotopes record a collapse of bioproductivity across the Cretaceous–Paleogene boundary in the Danish basin. Chemical Geology 654, 122058, https://doi.org/10.1016/j.chemgeo.2024.122058

Galehouse, J.S. 1971: Sedimentation analysis. In: Carver, R.E. (ed.): Procedures in sedimentary petrology, 69–94. London: Wiley.

Gilleaudeau, G.J., Voegelin, A.R., Thibault, N., Moreau, J., Ullmann, C.V., Klaebe, R.M., Korte, C. & Frei, R. 2018: Stable isotope records across the Cretaceous-Paleogene transition, Stevns Klint, Denmark: New insights from the chromium isotope system. Geochimica et Cosmochimica Acta 235, 305–332. https://doi.org/10.1016/j.gca.2018.04.028

Górka, H. 1957: Les Coccolithophoridés du Maestrichtien supérieur de Pologne. Acta Palaeontologica Polonica 2, 239–284.

Guerra, R. M., Concheyro, A., Kochhann, K. G. D., Bom, M. H. H., Ceolin, D., Musso, T., Savian, F.F. & Fauth, G. 2021: Calcareous microfossils and paleoenvironmental changes across the Cretaceous-Paleogene (K-Pg) boundary at the Cerro Azul Section, Neuquen Basin, Argentina. Palaeogeography, Palaeoclimatology, Palaeoecology 567, 110217. https://doi.org/10.1016/j.palaeo.2021.110217

Hansen, H.J. 1990: Diachronous extinctions at the K/T boundary – a scenario. In: Sharpton, V.L. & Ward, P.D. (eds): Global catastrophes in Earth history: An interdisciplinary conference on impacts, volcanism, and mass mortality. The Geological Society of America, Special Papers 247, 417–423. https://doi.org/10.1130/SPE247-p417

Hansen, T. 2019: Gastropods from the Cretaceous-Palaeogene boundary in Denmark. Zootaxa 4654, 196 pp. https://doi.org/10.11646/zootaxa.4654.1.1

Hart, M. B., Feist, S.E., Håkansson, E., Heinberg, C., Price, G.D., Leng, M.J., Watkinson, M.P. 2005: The Cretaceous-Palaeogene boundary succession at Stevns Klint, Denmark: Foraminifers and stable isotope stratigraphy. Palaeogeography, Palaeoclimatology, Palaeoecology 224, 6–26. https://doi.org/10.1016/j.palaeo.2005.03.029

Hashim, M.S. & Kaczmarek, S.E. 2021: Evolution of calcite microcrystal morphology during experimental dissolution. Journal Of Sedimentary Research 91, 229–242. https://doi.org/10.2110/jsr.2020.154

Heinberg, C. 1999: Lower Danian bivalves, Stevns Klint, Denmark: continuity across the K/T boundary. Palaeogeography, Palaeoclimatology, Palaeoecology 154, 87–106. https://doi.org/10.1016/S0031-0182(99)00088-7w

Heinberg, C. 2005: Morphotype biostratigraphy, diachronism, and bivalve recovery in the earliest Danian of Denmark. Bulletin of the Geological Society of Denmark 52, 81–95. https://doi.org/10.37570/bgsd-2005-52-07

Henehan, M.J., Hull, P.M., Penman, D.E., Rae, J.W. & Schmidt, D.N. 2016: Biogeochemical significance of pelagic ecosystem function: an end-Cretaceous case study. Proceedings of the Royal Society B: Biological Sciences 371, 20150510. https://doi.org/10.1098/rstb.2015.0510

Hildebrand-Habel, T. & Streng, M. 2003: Calcareous dinoflagellate associations and Maastrichtian-Tertiary climatic change in a high-latitude core (ODP Hole 689B, Maud Rise, Weddell Sea). Palaeogeography, Palaeoclimatology, Palaeoecology 197, 293–321. https://doi.org/10.1016/S0031-0182(03)00470-X

Hull, P. M. *et al.* 2020: On impact and volcanism across the Cretaceous-Paleogene boundary. Science 367, 266–272. https://doi.org/10.1126/science.aay5055

Jones, H.L., Lowery, C.M. & Bralower, T.J. 2019: Delayed calcareous nannoplankton boom-bust successions in the earliest Paleocene Chicxulub (Mexico) impact crater. Geology 47, 753–756. https://doi.org/10.1130/G46143.1

Kaczmarek, S.E., Fullmer, S.M. & Hasiuk, F.J. 2015: A universal classification scheme for the microcrystals that host limestone microporosity. Journal of Sedimentary Research 85, 1197–1212. https://doi.org/10.2110/jsr.2015.79

Katz, M.E., Finkel, Z.V., Grzebyk, D., Knoll, A.H. & Falkowski, P.G. 2004: Evolutionary trajectories and biogeochemical impacts of marine eukaryotic phytoplankton. Annual Review of Ecology, Evolution, and Systematics 35, 523–556. https://doi.org/10.1146/annurev.ecolsys.35.112202.130137

Knoll, A.H. & Follows, M.J. 2016: A bottom-up perspective on ecosystem change in Mesozoic oceans. Proceedings of the Royal Society B: Biological Sciences 283, 20161755. https://doi.org/10.1098/rspb.2016.1755

Machalski, M. & Heinberg, C. 2005: Evidence for ammonite survival into the Danian (Paleogene) from the Cerithium Limestone Member at Stevns Klint, Denmark. Bulletin of the Geological Society of Denmark 52, 97–111. https://doi.org/10.37570/bgsd-2005-52-08

MacLeod, K.G., Whitney, D.L., Huber, B.T. & Koeberl, C. 2007: Impact and extinction in remarkably complete Cretaceous-Tertiary boundary sections from Demerara Rise, tropical western North Atlantic. Geological Society of America Bulletin 119, 101–115. https://doi.org/10.1130/B25955.1

Mahanipour, A., Mutterlose, J. & Parandavar, M. 2022: Integrated bio- and chemostratigraphy of the Cretaceous – Paleogene boundary interval in the Zagros Basin (Iran, central Tethys). Palaeogeography, Palaeoclimatology, Palaeoecology 587, 110785. https://doi.org/10.1016/j.palaeo.2021.110785

Martinsson, A. 1970: Toponomy of trace fossils. In: Crimes, T.P. & Harper, J.C. (eds): Trace fossils. Geological Journal Special Issue 3, 323–330. Liverpool: Seel House Press.

McLachlan, S.M.S. & Pospelova, V. 2021: Calcareous dinoflagellate cyst distribution across the K/Pg boundary at DSDP site 577, Shatsky Rise, western North Pacific Ocean. Marine Micropaleontology 168, 102057. https://doi.org/10.1016/j.marmicro.2021.102057

Minoletti, F., de Rafelis, M., Renard, M., Gardin, S. & Young, J. 2005: Changes in the pelagic fine fraction carbonate sedimentation during the Cretaceous-Paleocene transition: contribution of the separation technique to the study of Bidart section. Palaeogeography, Palaeoclimatology, Palaeoecology 216, 119–137. https://doi.org/10.1016/j.palaeo.2004.10.006

Mohamed, O., Piller, W.E. & Egger, H. 2012: The dinocyst record across the Cretaceous/Palaeogene boundary of a bathyal mid-latitude Tethyan setting: Gosau Group, Gams Basin, Austria. Cretaceous Research 35, 143–168. https://doi.org/10.1016/j.cretres.2011.12.007

Nielsen, K.B. 1917: Cerithiumkalken i Stevns Klint. Danmarks

Geologiske Undersøgelse IV. Række, Vol. 1(7), 14 pp. https://doi.org/10.34194/raekke4.v1.6954

Obst, M., Wehrli, B. & Dittrich, M. 2009: $CaCO_3$ nucleation by cyanobacteria: laboratory evidence for a passive, surface-induced mechanism. Geobiology 7, 324–347. https://doi.org/10.1111/j.1472-4669.2009.00200.x

Ogg, J.G., Ogg, G.M. & Gradstein, F.M. 2016: A concise geologic time scale, 240 pp. Amsterdam: Elsevier.

Olsson, R.K., Berggren, W.A., Hemleben, C. & Huber, B.T. 1999: Atlas of Paleocene planktonic foraminifera. Smithsonian Contributions to Paleobiology 85, 1–252. https://doi.org/10.5479/si.00810266.85.1

Perch-Nielsen, K. 1968: Der Feinbau und die Klassifikation der Coccolithen aus dem Maastrichtien von Danemark. Biologiske Skrifter, Kongelige Danske Videnskabernes Selskab 16, 1–96.

Perch-Nielsen, K. 1979: Calcareous nannofossil zonation at the Cretaceous/Tertiary boundary in Denmark. In: Birkelund, T. & Bromley, R.G. (eds): Proceedings of the Cretaceous-Tertiary Boundary Events Symposium, 115–135. Copenhagen.

Rasmussen, H.W. 1971: Echinoid and crustacean burrows and their diagenetic significance in the Maastrichtian-Danian of Stevns Klint, Denmark. Lethaia 4, 191–216. https://doi.org/10.1111/j.1502-3931.1971.tb01289.x

Rasmussen, J.A., Heinberg, C. & Håkansson, E. 2005: Planktonic foraminifers, biostratigraphy and the diachronous nature of the lowermost Danian Cerithium Limestone Member at Stevns Klint, Denmark. Bulletin of the Geological Society of Denmark 52, 113–131. https://doi.org/10.37570/bgsd-2005-52-09

Reinhardt, P. & Górka, H. 1967: Revision of some Upper Cretaceous coccoliths from Poland and Germany. Neues Jahrbuch für Geologie und Paläontologie, Abhandlungen 129, 240–256.

Robbins, L.L. & Blackwelder, P.L. 1992: Biochemical and ultrastructural evidence for the origin of whitings – a biologically induced calcium-carbonate precipitation mechanism. Geology 20, 464–468. https://doi.org/10.1130/0091-7613(1992)020<0464:BAUEFT>2.3.CO;2

Romein, A.J.T. 1979: Lineages in Early Paleogene calcareous nannoplankton. Utrecht Micropaleontological Bulletin 22, 1–231.

Rosenkrantz, A. 1924: Nye Iagttagelser over Cerithiumkalken i Stevns Klint med Bemærkninger om Grænsen mellem Kridt og Tertiær. Meddelelser fra Dansk Geologisk Forening 6, 28–31.

Rosenkrantz, A. 1939: Faunaen i Cerithiumkalken og det hærdnede Skrivekridt i Stevns Klint. Meddelelser fra Dansk Geologisk Forening 9, 509–514.

Rosenkrantz, A., Surlyk, F., Anderskouv, K., Frykman, P., Stemmerik, L. & Thibault, N. 2021: The K-T boundary strata north of Korsnæb, Stevns Klint, Denmark – evolution and geometry revealed in a long, horizontal profile. Bulletin of the Geological Society of Denmark 69, 233–244. https://doi.org/10.37570/bgsd-2021-69-10

Schaefer, B. *et al.* 2020: Microbial life in the nascent Chicxulub crater. Geology 48, 328–332. https://doi.org/10.1130/G46799.1

Schmitz, B., Keller, G. & Stenvall, O. 1992: Stable isotope and foraminiferal changes across the Cretaceous Tertiary boundary at Stevns-Klint, Denmark – arguments for long-term oceanic instability before and after Bolide-Impact Event. Palaeogeography, Palaeoclimatology, Palaeoecology 96, 233–260. https://doi.org/10.1016/0031-0182(92)90104-D

Schoene, B., Eddy, M.P., Samperton, K.M., Keller, C.B., Keller, G., Adatte, T., Khadri, S.F.R. 2019: U-Pb constraints on pulsed eruption of the Deccan Traps across the end-Cretaceous mass extinction. Science 363, 862–866. https://doi.org/10.1126/science.aau2422

Schulte, P. *et al.* 2010: The Chicxulub asteroid impact and mass extinction at the Cretaceous-Paleogene boundary. Science 327, 1214–1218. https://doi.org/10.1126/science.1177265

Sepúlveda, J., Wendler, J.E., Summons, R.E. & Hinrichs, K.U. 2009: Rapid resurgence of marine productivity after the Cretaceous-Paleogene mass extinction. Science 326, 129–132. https://doi.org/10.1126/science.1176233

Sepúlveda, J., Alegret, L., Thomas, E., Haddad, E., Cao, C. & Summons, R.E. 2019: Stable isotope constraints on marine productivity across the Cretaceous–Paleogene mass extinction. Paleoceanography and Paleoclimatology 34, 1195–1217. https://doi.org/10.1029/2018PA003442

Shafik, S. & Stradner, H. 1971: Nannofossils from the Eastern Desert, Egypt. Jahrbuch der Geologischen Bundesanstalt, Sonderband 17, 69–104.

Smit, J. 2005: The section of the Barranco del Gredero (Caravaca, SE Spain): a crucial section for the Cretaceous/Tertiary boundary impact extinction hypothesis. Journal of Iberian Geology 31, 179–191.

Streng, M., Hildebrand-Habel, T. & Willems, H. 2004: A proposed classification of archeopyle types in calcareous dinoflagellate cysts. Journal of Paleontology 78, 456–483. https://doi.org/10.1666/0022-3360(2004)078<0456:APCOAT>2.0.CO;2

Suchéras-Marx, B., Mattioli, E., Allemand, P., Giraud, F., Pittet, B., Plancq, J. & Escarguel, G. 2019: The colonization of the oceans by calcifying pelagic algae. Biogeosciences 16, 2501–2510. https://doi.org/10.5194/bg-16-2501-2019

Surlyk, F. 1997: A cool-water carbonate ramp with bryozoan mounds: Late Cretaceous-Danian of the Danish basin. In: James. N.P. & Clarke, J.A.D. (eds): Cool-Water Carbonates. SEPM Special Publication 56, 293–307. https://doi.org/10.2110/pec.97.56.0293

Surlyk, F. & Lykke-Andersen, H. 2007: Contourite drifts, moats and channels in the Upper Cretaceous chalk of the Danish Basin. Sedimentology 54, 405–422. https://doi.org/10.1111/j.1365-3091.2006.00842.x

Surlyk, F., Damholt, T. & Bjerager, M. 2006: Stevns Klint, Denmark: Uppermost Maastrichtian chalk, Cretaceous-Tertiary boundary, and lower Danian bryozoan mound complex. Bulletin of the Geological Society of Denmark 54, 1–48. https://doi.org/10.37570/bgsd-2006-54-01

Thierstein, H.R. 1980: Selective dissolution of late cretaceous and earliest tertiary calcareous nannofossils: Experimen-

tal evidence. Cretaceous Research 1, 165–176. https://doi.org/10.1016/0195-6671(80)90023-3

Thompson, J.B. 2000: Microbial whitings. In: Riding, R.E. & Awramik, S.M. (eds): Microbial Sediments, 250–260. Berlin: Springer. https://doi.org/10.1007/978-3-662-04036-2_27

Varol, O. 1989: Palaeocene calcareous nannofossil biostratigraphy. In: Crux, J.A. & van Heck, S.E. (eds): Nannofossils and their applications, 267–310. British Micropalaeontological Society.

Vekshina, V.N. 1959: Coccolithophoridae of the Maastrichtian deposits of the West Siberian lowlands. Siberian Science Research Institute of Geology, Geophysics, Mineralogy and Raw Materials 2, 56–81.

Wendler, J. & Willems, H. 2002: Distribution pattern of calcareous dinoflagellate cysts across the Cretaceous-Tertiary boundary (Fish Clay, Stevns Klint, Denmark): Implications for our understanding of species-selective extinction. In: Koeberl, C. & MacLeod, K.G. (eds): Catastrophic events and mass extinctions: Impacts and beyond. Geological Society of America, Special Papers 356, 265–275. https://doi.org/10.1130/0-8137-2356-6.265

Westerhold, T. *et al.* 2020: An astronomically dated record of Earth's climate and its predictability over the last 66 million years. Science 369, 1383-1387. https://doi.org/10.1126/science.aba6853

Wilson, J.L. 1975: Carbonate facies in geologic history, 471 pp. Berlin: Springer. https://doi.org/10.1007/978-1-4612-6383-8

Zachos, J.C. & Arthur, M.A. 1986: Paleoceanography of the Cretaceous/Tertiary boundary event: Inferences from stable isotopic and other data. Paleoceanography 1, 5–26. https://doi.org/10.1029/PA001i001p00005